Theoretical study of the effect of π^+-π^+ association in imidazolium ionic liquids at charged interfaces

Ke Ma*
School of Materials Science and Engineering, Tianjin University of Technology, Tianjin 300384, P. R. China and Tianjin Key Laboratory for Photoelectric Materials and Devices, Tianjin University of Technology, Tianjin 300384, China

Jan Forsman
Theoretical Chemistry, Chemical Centre, Lund University, P. O. Box 124, S-221 00 Lund, Sweden

Clifford E. Woodward†
School of Physical, Environmental and Mathematical Sciences, University of New South Wales, Canberra at the Australian Defence Force Academy, Canberra ACT 2600, Australia
(Received 24 May 2017; published 18 December 2017)

We develop an extended classical density-functional theory to describe clustering of imidazolium-based cations into linear chains, driven by π-π stacking. We find that the associating system displays a similar short-ranged structure to the completely dissociated fluid. We also construct a restricted primitive model for associating ionic species in an RTIL+solvent mixture. The double-layer formed in these systems exhibits strong overscreening by the cation chains, as expected. Significantly enhanced capacitance is also observed for the case where counterions are the associating species. The established density-functional method can be also used to describe polydisperse polyelectrolyte models.

DOI: 10.1103/PhysRevE.96.062609

I. INTRODUCTION

Room-temperature ionic liquids (RTILs) are often thought to display association of oppositely charged ions to form ion pairs as a natural consequence of strong electrostatic correlations. In recent work, we used classical density-functional theory (DFT) to investigate the role played by ion pairing and neutral clusters on the properties of RTILs at electrified interfaces [1,2]. However, there is also mounting evidence that like-charged ions may also associate, e.g., the occurrence of π-π stacking of imidazolium cations has been implicated in NMR measurements [3–5] and also in recent *ab initio* calculations [6]. The physical π-π interaction between the ionic liquid and multiwall carbon nanotubes has been investigated with Raman spectroscopy [7] and single-crystal x-ray structure of a palladium(II) coordination complex [8]. This π-π stacking can minimize the expansion of metal-ligand bonds within complexes, which optimizes the performance of light-emitting electrochemical cells [9]. Better analyte transport properties of ionic liquid micelles are also attributed to π-π as well as hydrophobic interactions [10].

Theoretical studies using *ab initio* molecular dynamics (MD) simulations have uncovered characteristic conformations of neighboring imidazolium cations which are stacked directly on top of each other [11]. The presence of anions at the periphery helps to stabilize the π-π stacking conformation [12]. It was found that the thiocyanate (SCN) anion was particularly effective at stabilizing π-π stacked 1-ethyl-3-methylimidazolium cations due to their small size hydrogen bonding ability [13]. Pair distributions obtained from MD simulations indicate that the center-to-center distance between stacked imidazolium cations is typically around 0.4 nm [14]. In aqueous solutions, the stacked structure is enhanced by the hydrophobic effect and further facilitated by the screening of charge repulsions by the solvent. Mele *et al.* [15] have studied cation–cation distances in neat imidazolium-based RTILs using nuclear magnetic resonance (NMR) spectroscopy. Nuclear Overhauser effect (NOE) contacts between π-π stacked cations, obtained by two-dimensional (2D) NMR, suggests that like-charged interactions are also adequately screened in pure RTILs, which is not surprising, given the very short Debye length in these fluids. Furthermore, various motifs of ion pairs and clusters were explored as stable structures in simulations of RTILs which included associated cations formed from π-π stacking [16]. It is therefore of interest to extend our previous DFT studies to include the effect of association between cations.

Density-functional theory has been used for many years to predict the hard-sphere structure at surfaces for simple and complex fluids [17–19] and more recently for RTILs [20,21]. Over time, DFT has become an accurate and complementary tool, along with molecular simulations for interfacial systems under external potentials [22–26]. The development of analytic methods for dealing with ideal clusters has obviated the need to use simulations, such as Monte Carlo (MC), in order to enumerate configurations within a self-consistent field [27,28] allowing instead numerical solutions on a spatial grid (at least for simple geometries).

In our approach, the cluster population in the bulk fluid with which the nonuniform fluid is in equilibrium is set *a priori*. In contrast to the spherical or globular-shaped clusters that we have dealt with in previous work [1,2], it is expected that π-π stacking of cations will lead to linear chains of associated molecules instead. Hence, they resemble a *living* linear polyelectrolyte, wherein cationic "monomers" can freely associate or dissociate from the chain (while Coulombic repulsions are

*kema@tjut.edu.cn
†c.woodward@adfa.edu.au

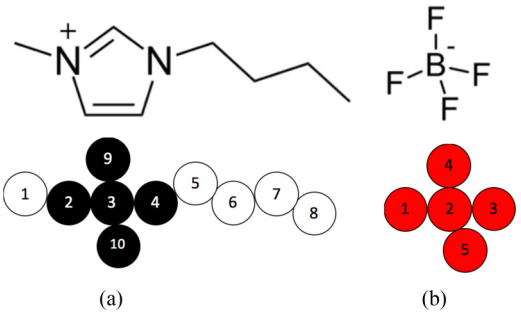

FIG. 1. Coarse-grained model of (a) cation $[C_4MIM^+]$ and (b) anion $[BF_4^-]$. Black spheres represent positively charged beads while white spheres represent neutral beads on the cation. Red spheres represent negatively charged beads on the anion.

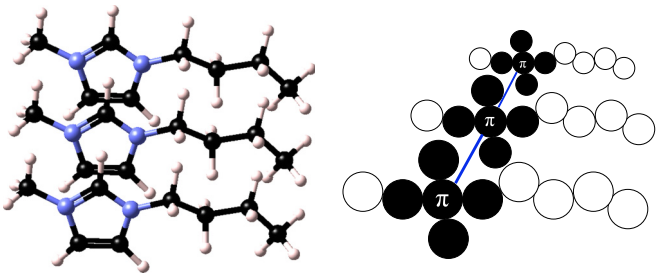

FIG. 2. Schematic representation of the three stacked imidazolium cations in the left. On the right is the model of associating cation chain of length $L = 3$; the central bead on each cation becomes the repeating π bead and is bonded to another at a fixed distance of σ.

presumably screened by accompanying molecular anions). The molecular-weight distribution of the cationic polymer is expected to be exponential, provided there is sufficient screening of the intramolecular charge. While this model for imidazolium-based RTILs remains speculative, it is of interest to explore its properties, even from an academic point of view. For example, the asymmetry induced by different molecular architectures of anions and cations in RTILs in general will be enhanced by the presence of cation association. Furthermore, it has been shown in previous work [29] that equilibrium polymers can undergo adsorption transitions in the presence of sufficiently attractive surfaces. This phenomenon may lead to interesting electrodic properties in RTILs which display cation association.

A classical DFT theory that describes the reversible association of monomers into linear chains has been developed by Woodward and Forsman and applied to a number of problems [30]. The theory is a subset of a more general DFT approach to polydisperse polymers whose molecular weight profile is given by the well-known Schultz–Flory distribution. The lowest order Schultz–Flory distribution is exponential and describes the living polymer case. Below, we describe a DFT treatment of associating linear chains of cations, assuming a relatively complex multibranched architecture for the imidazolium cation. We also consider a much simpler restricted primitive model for the RTIL. These ions are assumed to be immersed in an implicit solvent, with a given dielectric constant. We continue to use the term polymer, or oligomer, as an "analog" for the associating complex of the RTIL model. This system focuses on RTIL solution in the presence of charged electrodes, wherein we find an enhanced surface adsorption of the cationic polymer, giving rise to novel properties of the ionic liquid at an electrode.

II. DENSITY-FUNCTIONAL THEORY FOR AN RTIL WITH LINEARLY ASSOCIATING CATIONS

A. Coarse-grained model

Here we use a simple coarse-grained model for 1-alkyl-3-methyl imidazolium tetrafluroborate RTILs with the general formula $[C_nMIM^+][BF_4^-]$ [1]. The case, $n = 4$, 1-butyl-3-methyl imidazolium tetrafluroborate, is depicted in Fig. 1. In our model, both cation and anion species consist of tangentially connected hard spheres with equal diameters, where each sphere can roll over the surface of their bonded neighbors. A sphere diameter of $\sigma = 2.4$ Å, is used, which is consistent with the actual molecular volumes of both anions and cations. The imidazolium ring is modeled as a five bead star, where each sphere in the star carries a partial charge of $+0.2e$. The methyl groups are modeled as neutral spheres. A star of five beads (each carrying charge of $-0.2e$) is used to model $[BF_4^-]$. The electrostatic interaction between charges is screened by a relative dielectric constant, ϵ_r, which accounts for electronic and intramolecular polarizability. A value of $\epsilon_r = 2.3$ is used, which is typical for hydrocarbon groups. Finally, all beads are also assumed to interact via a long-range attractive component that has a Lennard–Jones (LJ) form,

$$\Phi_{\rm att}(r) = -4\epsilon_{\rm LJ}\left(\frac{\sigma}{r}\right)^6. \quad (1)$$

We used $\epsilon_{\rm LJ}/k_B = 100$ K, where k_B is Boltzmann's constant and $\sigma = 2.4$ Å is the same as the hard-sphere diameter of the beads.

B. Free-energy functional

Using this coarse-grained model, we include π-π stacking between cations using a similar device to what was used in our modeling of clusters [1,2]. That is, the *reversibly* associating fluid is treated as a collection of different species determined by a chemical potential, which implicitly contains a free energy of association. The association between two cations is modeled as a rigid bond of length σ between the central beads of the charged star on each of the cations. The central bead is labeled 3 in Fig. 1(a). This gives rise to intermolecular "bonding" which is essentially identical in form to the intramolecular bonding. We note here that π-π stacking will generally give rise to an internal "stiffness" in the system, which will not be accurately reflected in the current model. We note, however, that stiffness effects are possible to include within the density-functional treatment but will not be considered here. Previous work has shown that predictions that follow from the density-functional theory applied to molecular clusters are qualitatively (and even quantitatively) independent of the bonding description between associating species, provided they are sensible [1,2]. The π-π association will give a distribution of cationic chains, with different lengths L. A sequence of three such associated cations is depicted in Fig. 2. While there is good experimental

evidence for π-π association, the expected average sizes of the short polymers or oligomers is still largely unknown. Thus the average length, $\langle L\rangle_b$, of the clusters in the bulk solution will be treated as a variable in the following analysis. The free-energy density functional will include these linear chains and can be written as

$$\begin{aligned}\Omega = {} & F^{\rm id}[\{N^{(\alpha)}(\mathbf{R}^\alpha)\}] + F_{\rm hs}[n_s(\mathbf{r})] \\ & + F_{\rm disp}[n_s(\mathbf{r})] + F_{\rm corr}[n_c(\mathbf{r}),n_a(\mathbf{r})] \\ & + F^{\rm el}_{\rm surf}[n_c(\mathbf{r}),n_a(\mathbf{r})] + F^{\rm disp}_{\rm surf}[n_s(\mathbf{r})] \\ & - \sum_\alpha (\mu_\alpha + q_\alpha \Psi_D)\int N_\alpha(\mathbf{R}^\alpha) d\mathbf{R}^\alpha, \end{aligned} \tag{2}$$

where μ_α is the species chemical potential and Ψ_D is the Donnan potential, which maintains electroneutrality in the system, in which all quantities can be categorized into ideal term and excess free-energy terms [1,2]. The different terms appearing in the functional will be described below. Here the superscript α enumerates all species present, i.e., anions ($\alpha = a$), as well as the cationic chains of different length L ($\alpha = \{c^L; L = 1,2,\ldots,\infty\}$). The superscript α is also used to label the coordinates of the complex species, e.g., quantity, $\mathbf{R}^{c^L}$, represents the site coordinates of the beads in a cation chain of length L.

With this nomenclature, the ideal term of the free energy is given by

$$\begin{aligned}&\beta F^{\rm id}[\{N^{(\alpha)}(\mathbf{R}^\alpha)\}] \\ &= \sum_{\alpha=a,\{c^L;L=1,\infty\}} \int N^{(\alpha)}(\mathbf{R}^\alpha)(\ln[N^{(\alpha)}(\mathbf{R}^\alpha)] - 1) d\mathbf{R}^\alpha \\ &\quad + \sum_\alpha \int N^{(\alpha)}(\mathbf{R}^\alpha)\beta V_B^{(\alpha)}(\mathbf{R}^\alpha)\, d\mathbf{R}^\alpha. \end{aligned} \tag{3}$$

Here $V_B^{(\alpha)}(\mathbf{R}^\alpha)$ is the bonding function and will include a combination of intra- and intermolecular rigid bonds, depending on the species. The probability distribution of cation chain lengths in the bulk, denoted by $F(L)$, is determined by the chemical potential μ_{c^L}. This is a function of the strength of the π-π stacking interaction and we expect it to lead to an exponential form for $F(L)$. For the moment, however, we will just assume a general representation, to obtain

$$\beta\mu_{c^L} = \ln[\phi_p F(L)], \tag{4}$$

where ϕ_p is the average bulk density of the cationic living polymers, formed by their association (including single cations). Note that ϕ_p is not equal to the total bulk density of cations, which is instead given by $n_b^{(c)} = \sum_{L=1}^\infty \phi_p L F(L) = \phi_p \langle L\rangle_b$, where $\langle L\rangle_b$ is the average length of the associated chains in the bulk.

The *collective site densities* are denoted as $\{n_\beta(\mathbf{r}); \beta = c,a,n\}$, which correspond to the sum over site densities of the same type, e.g., positive (c), negative (a), and neutral (n) beads, respectively. Hence we have

$$n_\beta(\mathbf{r}) = \sum_\alpha \sum_{i(\beta)} n_i^{(\alpha)}(\mathbf{r}), \tag{5}$$

where the nomenclature of the sum over i implies that we sum over all sites of type β in the species α. The specific site i density in the species α is given by

$$n_i^{(\alpha)}(\mathbf{r}) = \int \delta(\mathbf{r} - \mathbf{r}_i) N^{(\alpha)}(\mathbf{R}^\alpha)\, d\mathbf{R}^\alpha, \tag{6}$$

where $\delta(\mathbf{r})$ is the Dirac δ function. The *total* site density is given by $n_s(\mathbf{r}) = n_c(\mathbf{r}) + n_a(\mathbf{r}) + n_n(\mathbf{r})$.

The excess free-energy terms (beyond the ideal contribution) are assumed to depend only on the site densities. The quantity $F_{\rm hs}[\bar{n}_s(\mathbf{r})]$, accounts for the entropy arising from the hard-sphere interaction between all beads [23]. This term is derived from the generalized Flory-dimer (GF-D) equation of state [23], which is assumed to be a functional of the weighted bead density $\bar{n}_s(\mathbf{r})$ [17],

$$\bar{n}_s(\mathbf{r}) = \frac{3}{4\pi\sigma^3}\int_{|r-r'|<\sigma} n_s(\mathbf{r}')\, d\mathbf{r}'. \tag{7}$$

The nonelectrostatic attractive interactions between beads is obtained as an integral over the truncated LJ potential, $\Phi_{\rm att}(r)$, which was described earlier, Eq. (1),

$$F_{\rm disp}[n_s(\mathbf{r})] = \frac{1}{2}\iint_{|\mathbf{r}-\mathbf{r}'|\geqslant\sigma} n_s(\mathbf{r}) n_s(\mathbf{r}')\Phi_{\rm att}(|\mathbf{r}-\mathbf{r}'|)\, d\mathbf{r}\, d\mathbf{r}'. \tag{8}$$

The electrostatic interactions between charged sites are obtained using a correlation kernel, which extends the mean-field approach, inherent to the Poisson-Boltzmann approximation

$$\begin{aligned} F_{\rm corr} &\approx \frac{1}{2}\iint \sum_{\beta=a,c}\sum_{\beta'=a,c} n_\beta(\mathbf{r}) n_{\beta'}(\mathbf{r}') K^{\rm corr}_{\beta\beta'}(|\mathbf{r}-\mathbf{r}'|)\, d\mathbf{r}\, d\mathbf{r}' \\ &= F^{\rm el}_{\rm like} + F^{\rm el}_{\rm unlike}, \end{aligned} \tag{9}$$

where $n_\beta(\mathbf{r})$ is the total density of sites carrying a charge of type $\beta = (a,c)$. The algebraic form of the overall *correlation kernels*, $K^{\rm corr}_{\beta\beta'}$, depends on whether one is treating like or unlike Coulombic interactions. In the case of like charges, we have

$$\begin{aligned} F^{\rm el}_{\rm like} = {} & \frac{1}{2}\iint \sum_{\beta=a,c} n_\beta(\mathbf{r}) n_\beta(\mathbf{r}') H_\beta(|\mathbf{r}-\mathbf{r}'|) \\ & \times \Phi^{\rm el}_{\beta\beta}(|\mathbf{r}-\mathbf{r}'|)\, d\mathbf{r}\, d\mathbf{r}', \end{aligned} \tag{10}$$

where $\Phi^{\rm el}_{\beta\beta'}(|\mathbf{r}-\mathbf{r}'|)$ is the Coulomb potential between a pair of charged sites of type β and β', i.e.,

$$\Phi^{\rm el}_{\beta\beta'}(r) = \frac{1}{4\pi\epsilon_0\epsilon_r}\frac{z_\beta z_{\beta'}}{r}, \tag{11}$$

where z_β is the charge of site β, ϵ_0 is the permittivity of vacuum, and ϵ_r is the relative permittivity (as mentioned earlier, we use $\epsilon_r = 2.3$). The function $H_\beta(|\mathbf{r}-\mathbf{r}'|)$ describes an exponential "Coulomb hole,"

$$H_\beta(r) = 1 - e^{-\lambda_\beta r}. \tag{12}$$

The parameter λ_β is determined such that the "Coulomb hole" describes self-exclusion over the whole space. That is,

$$n^b_\beta \int \{H_\beta(|\mathbf{r}|) - 1\}\, d\mathbf{r} = -1, \tag{13}$$

where n_β^b is the bulk density of the site β. This gives

$$\lambda_\beta = \frac{\sqrt{2}}{s_\beta} \tag{14}$$

with

$$s_\beta = \left[\frac{3}{4\pi n_\beta^b}\right]^{1/3}. \tag{15}$$

For unlike–charge interactions between anions and cations,

$$F_{\text{unlike}}^{\text{el}} = \frac{1}{2}\iint \sum_{\beta\neq\beta'=a,c} n_\beta(\mathbf{r}) n_{\beta'}(\mathbf{r}')\Theta(|\mathbf{r}-\mathbf{r}'|-d) \times \Phi_{\beta\beta'}^{\text{el}}(|\mathbf{r}-\mathbf{r}'|)d\mathbf{r}d\mathbf{r}', \tag{16}$$

where the Heaviside function is defined as $\Theta(x) = 1$ for $x > 0$ and $\Theta(x) = 0$ for $x \leqslant 0$. The parameter $d = \chi\sigma$ mimics the enhanced correlation between oppositely charged species (not in the same cluster) and provides the only adjusted parameter in the model. It is fitted to give the correct bulk ion density for the particular RTIL at a given pressure and temperature.

Finally, $\Phi(\mathbf{R}^\alpha)$ is the external potential acting on the species α. In the systems studied here, this will be due to charged planar surfaces, modeling electrodes. We will assume the surfaces are smooth planes represented as infinite half-spaces of Lennard–Jones particles, which interact with all fluid molecules. Thus, the total dispersion energy due to each bead interacting with the surface is given by

$$F_{\text{surf}}^{\text{disp}} = \int_0^\infty \omega_{\text{LJ}}(z) n_s(z)\, dz, \tag{17}$$

where $n_s(z)$ is the total averaged site density, which is a function of the perpendicular distance to the surface, z. $\omega_{\text{LJ}}(z)$ is obtained by integrating the 12-6 LJ potential over the whole surface,

$$\omega_{\text{LJ}}(z) = 4\pi\epsilon_{\text{LJ}}\rho_s\sigma^2\left[\frac{1}{5}\left(\frac{\sigma}{z}\right)^{10} - \frac{1}{2}\left(\frac{\sigma}{z}\right)^4\right]. \tag{18}$$

For simplicity, we use the same strength and range of interaction as the dispersion force between beads, see Eq. (1). The surfaces are charged and hence will interact with charged sites in the fluid molecules. We make the simple choice that the relative dielectric constant, ϵ_r, is constant throughout all space (including within the surfaces), so image effects are not considered. Thus the electrostatic interaction between the fluid and surface is simply given by

$$F_{\text{surf}}^{\text{el}} = \iint \sum_{\beta=a,c} n_\beta(\mathbf{r}) \frac{1}{4\pi\epsilon_0\epsilon_r} \frac{z_\beta \Sigma(\rho)}{|\mathbf{r}-\rho|} d\mathbf{r}d\rho, \tag{19}$$

where $\Sigma(\rho)$ is the surface charge density and ρ is a two-dimensional surface vector.

C. Solving for the site densities

The minimization of the free-energy functional, leads to explicit expressions for the oligomeric distributions $N^{(\alpha)}(\mathbf{R}^\alpha)$. We will focus here on the cationic chains as these present the more difficult calculation. The determination of the anion bead densities follows from the analysis presented below in a reasonably straightforward way.

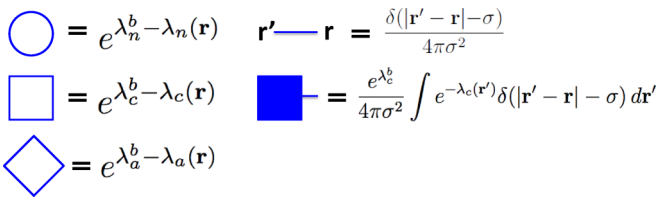

FIG. 3. Diagrams of bonds and vertices with circle for neutral, square for positive, and diamond for negative beads in the model. Vertices stand for local excess chemical potential factors. The solid line represents the rigid bond between neighboring beads. Color in a vertex means integrating the vertex's coordinate over all space. An example is given of integrating a positive bead with a bond end at $\mathbf{r}$.

For a chain of L associated cations, minimization of the free energy gives

$$N^{(c^L)}(\mathbf{R}^{c^L}) = \phi_p F(L) \exp\left\{-\beta V_B^{(c^L)}(\mathbf{R}^{c^L}) + \sum_j \left[\lambda^{(c^L),b} - \lambda_j^{(c^L)}(\mathbf{r}_j)\right]\right\}. \tag{20}$$

We recall that the intermolecular association linking the cations is implicitly contained in the bonding potential, $V_B^{(c^L)}(\mathbf{R}^{c^L})$. Thus, the Boltzmann factor containing the bonding term will give rise to a product of Dirac δ functions, which reflects the topology of the cationic chain, i.e.,

$$\exp\left[-\beta V_B^{(c^L)}(\mathbf{R}^{c^L})\right] = \prod_{\langle i,j\rangle} \frac{\delta(|\mathbf{r}_i - \mathbf{r}_j| - \sigma)}{4\pi\sigma^2}, \tag{21}$$

where $\langle i,j\rangle$ represent all bonded pairs (both intra- and intermolecular) in the cluster.

Each specific site j on the species c^L carries an excess chemical potential $\lambda_j^{(c^L),b} - \lambda_j^{(c^L)}(\mathbf{r})$, where

$$\lambda_j^{(c^L)}(\mathbf{r}) = \frac{\delta\beta F^{\text{ex}}}{\delta n_j^{(c^L)}(\mathbf{r})} \tag{22}$$

with F^{ex} the sum of all the excess free-energy terms, beyond the ideal contribution, and $n_j^{(c^L)}(\mathbf{r})$ are the site densities from Eq. (6). Equations (20)–(22) need to be solved self-consistently, as the $\lambda_j^{(c^L)}(\mathbf{r})$ themselves are functionals of the site densities.

The evaluation of the site densities can be facilitated using diagrammatic methods. We define a set of vertices and bonds, as shown in Fig. 3. The open symbols in the shapes of circle, square, and diamond, correspond to the neutral, cationic, and anionic factors, respectively, containing the corresponding excess chemical potential terms (as indicated). In defining these we note that, with the form of the free-energy functional used here, the excess chemical potential $\lambda_j^{(\alpha)}(\mathbf{r})$ is independent of species type α and depends only on the site type of j. That is, $\lambda_j^{(\alpha)}(\mathbf{r}) = \lambda_\beta(\mathbf{r})$ if the site j is of type β, as defined earlier.

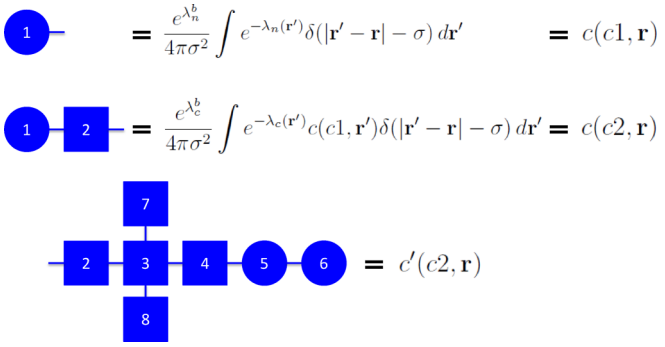

FIG. 4. Diagrams for the recursive process of generating branch end segment distribution, $c(c2,\mathbf{r})$ from $c(c1,\mathbf{r})$. Example of the complementary end segment distribution $c'(c2,\mathbf{r})$ for $[C_2MIM^+]$.

Equation (22) can then be written as

$$\lambda_\beta(\mathbf{r}) = \frac{\delta\beta F^{\text{ex}}}{\delta n_\beta(\mathbf{r})}, \tag{23}$$

where $n_\beta(\mathbf{r})$ is the collective density of sites of type β, as defined earlier. The bulk values of these excess chemical potentials are denoted as λ_β^b. The solid line in Fig. 3 represents the normalized Dirac δ function, describing the freely rotating rigid bond between sites. Graphs consisting of vertices connected by bonds represent the product of the associated functions. Color in a vertex indicates integrating that site over all space, as shown in Fig. 3.

The sites of the cationic and anionic molecules are denoted as $(c1,c2\ldots)$ and $(a1,a2\ldots)$; see Fig. 4 for examples of the site numbering of $[C_2MIM^+]$. In that figure we have also given a few examples of so-called *segment densities*. These correspond to graphs of a connected subset of colored vertices (corresponding to the molecular sites on individual anion and cation species) with a dangling bond. It is useful to define two classes of these segment densities. One we will call *branch* segment densities denoted as $c(i,\mathbf{r})$. These contain only one terminal site of the molecule (a site with only a single incident bond) and a dangling rigid bond attached at site i. The other class we will call *complementary* segment densities, denoted as $c'(i,\mathbf{r})$. These are also connected graphs of colored vertices at least one of which is a branching site, i.e., a site with more than two adjacent bonds (e.g., $c3$ on the cation is a branching site) and a dangling bond attached at site i. If a molecule has a single branching site, then the vertices in the molecule which are *not* included in the complementary graph can be connected and colored to make a branch segment distribution. Examples of $c(c2,\mathbf{r})$ and $c'(c2,\mathbf{r})$ are given in Fig. 4.

The advantage of defining branch segment distributions is that they can be obtained recursively along each branching chain, which saves the numerical effort for molecules with long branches. For example, we have

$$c(c1,\mathbf{r}) = \frac{e^{\lambda_n^b}}{4\pi\sigma^2}\int e^{-\lambda_n(\mathbf{r})}\delta(|\mathbf{r}'-\mathbf{r}|-\sigma)\,d\mathbf{r}'. \tag{24}$$

The function $c(c2,\mathbf{r})$ is then generated from $c(c1,\mathbf{r})$, as illustrated in Fig. 4, according to the recursion formula

$$c(c2,\mathbf{r}) = \frac{e^{\lambda_c^b}}{4\pi\sigma^2}\int c(c1,\mathbf{r}')e^{-\lambda_c(\mathbf{r}')}\delta(|\mathbf{r}'-\mathbf{r}|-\sigma)\,d\mathbf{r}'. \tag{25}$$

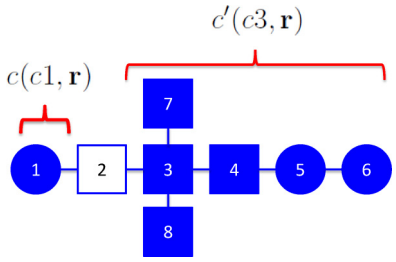

FIG. 5. Diagram for normalized site density of bead $c2$ on cation $[C_2MIM^+]$. End segment distribution $c(c1,\mathbf{r})$ and $c'(c3,\mathbf{r})$ are combined.

On the other hand, *complementary* segment distributions are more complex and must be constructed (usually by inspection) from a collection of branch segment distributions. For example, the complementary graph $c'(c3,\mathbf{r})$ can be obtained from branch segment distributions as follows:

$$c'(c3,\mathbf{r}) = \frac{e^{\lambda_c^b}}{4\pi\sigma^2}\int e^{-\lambda_c(\mathbf{r}')}c(c4,\mathbf{r}')c(c7,\mathbf{r}') \times c(c8,\mathbf{r}')\delta(|\mathbf{r}'-\mathbf{r}|-\sigma)\,d\mathbf{r}'. \tag{26}$$

Any site density for free cations and anions can always be obtained using a product of a site vertex and adjacent branch and complementary segment distributions. For example, the graph in Fig. 5 represents the normalized site density,

$$n_{c2}^{(c)}(\mathbf{r})/n_b^{(c)} = e^{\lambda_c^b-\lambda_c(\mathbf{r})}c(c1,\mathbf{r})c'(c3,\mathbf{r}), \tag{27}$$

where $n_b^{(c)}$ is the bulk density of free cations. The density contribution due to all other sites on free cations and anions can be calculated in a similar fashion.

In principle, obtaining the contribution to a particular site density from a chain of associated cations of given length L could proceed by direct evaluation of Eqs. (6) and (20). However, solving for each chain length one by one is impractical, given that there are essentially an infinite number of different lengths. It is possible to simplify the calculation given that we need only to find the total site densities of particular type ($\beta = a,c,n$), which involves summing over all chain lengths. The form of Eq. (20) implies that this sum corresponds to averaging over the distribution $F(L)$. Fortunately, it is possible to solve this problem, which we will demonstrate in the Appendix sections for the case of $[C_4[MIM^+]$ cation association. We will use the site numbering as suggested in Fig. 1.

III. RESULTS: STRUCTURAL PROFILES

Using this distribution we solve the DFT for the case of a pure RTIL between two charged planar surfaces, allowing for cation association. We chose $\langle L\rangle_b = 5$, which corresponds to a rather strong π-π interaction. Consistent with the established $[C_4MIM^+][BF_4^-]$ model [1], the bulk ionic density (either anions or cations) is given by $n_b\sigma^3 = 0.04475$ and the inverse surface charge density was $a_s = -320$ Å$^2/e$. In this study, we will compare the structural profiles of the π-π associating ionic liquid with the fluid where we assume association does not occur.

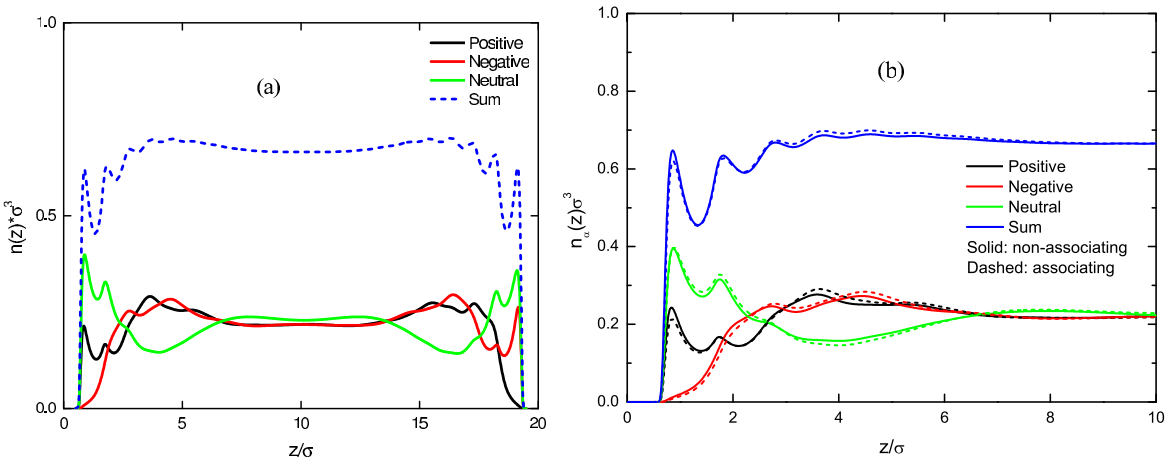

FIG. 6. Density profiles from the DFT for $[C_4MIM^+][BF_4^-]$ between two oppositely charged surfaces (left surface at -320 Å$^2/e$ while right surface at $+320$ Å$^2/e$), (a) density profiles of positive, negative, neutral beads and their sum in the associating cation system; (b) comparison of associating cation system with nonassociating cation system near negative surface in the left.

In Fig. 6(a), we show the density profiles for the associating fluid in the presence of the two oppositely charged surfaces. This system approximates a negatively charged electrode pore, immersed in the ionic liquid. It is in this situation that we may have expected to see a large effect due to the association of cations, driven by the negative surface charge. However, we find that the density profile of the associating cations does not significantly differ from that of the nonassociating ionic liquid, as is shown in Fig. 6(b). In fact, if anything, the (associating) cation density is slightly lower at the surfaces, compared with the nonassociating case, presumably due to depletion effects on the effective cationic polymer chains. This minor effect notwithstanding, the overall results are remarkably similar to what was seen in our study of ion pairs and neutral clusters formed by RTILs, which were also shown to be in excellent agreement with Monte Carlo simulations of the identical model [1]. In both cases, it seems that the fluid tends to compensate for the presence of associated species, to give very similar density profiles no matter what clustering is present. That is, in the dense, neat ionic liquid, close association of particles is present in any case due to strong electrostatic correlations. So additional correlations, say via a π-π association mechanism, has little additional affect on the overall structure. Variations in density profiles are also constrained by electroneutrality, whereby the response of the fluid to an applied surface charge has to satisfy the requirement of zero net charge in the overall system.

IV. RTIL + SOLVENT MIXTURES: A RESTRICTED PRIMITIVE MODEL WITH CATION ASSOCIATION

While it is possible to explore more of the parameter space of the neat ionic liquid, it was apparent to us that the qualitative findings for the structural profiles would be more or less similar to what we have already observed, according to the discussion above. Instead, we expected that a more dramatic effect due to ion association would be apparent in RTIL solutions, wherein the overall ionic liquid concentration is relatively low. Hence, instead of a pure RTIL, we turned our attention to an RTIL+solvent mixture. The inclusion of a solvent can be instrumental in promoting stronger cation–cation attractions via, say, hydrophobic interactions (for aqueous solvents) while keeping charge–charge repulsion screened with a large dielectric constant. Dilute solutions of RTILs have been known to undergo surface phase transitions under certain circumstances, driven by strong interactions within RTILs [31]. For example, huge increases in capacitance have been observed in RTIL solutions wherein the ionic liquid component condenses on the surface of an electrode in a wetting transition [31]. This gives rise to large fluctuations in the component fractions of the solution near the charged surface. Similar behavior is seen in RTIL solutions in contact with porous media. In this case, capillary condensation can cause large changes in the differential capacitance [31]. The presence of charged equilibrium chains arising from associative π-π stacking may allow the system to undergo an adsorption transition at the surface of electrodes, similarly to what is seen in neutral polymers at sufficiently attractive surfaces [29].

In an effort to simplify the calculations, we explored a model with reduced complexity, as the qualitative physics should not be too different provided the basic features of an ionic liquid solution are retained. To this end we note that a solution of an ionic liquid in fact differs little from that of a standard electrolyte, apart from the already-described molecular anisotropy. However, the latter should not affect too greatly the nature of the surface adsorption transition when π-π association is present. Furthermore, while distributed charges were necessary in the model of Fig. 1 (in order to prevent crystallization), such is not the case for a dilute solution. These considerations prompted us to implement the simple restricted primitive model (RPM) as a model for the RTIL in the following adsorption studies, augmented by an additional π-π interaction potential, allowing cation association. In the RPM, anions and cations are modelled as simple charged hard spheres, both with the same diameter σ, while the solvent is treated *implicitly* so that its presence is only felt via the relative dielectric constant.

As the solvent is treated implicitly, the free-energy functional for the RTIL+solvent mixture has essentially the same structure as given in Eq. (2) above. A significant simplification

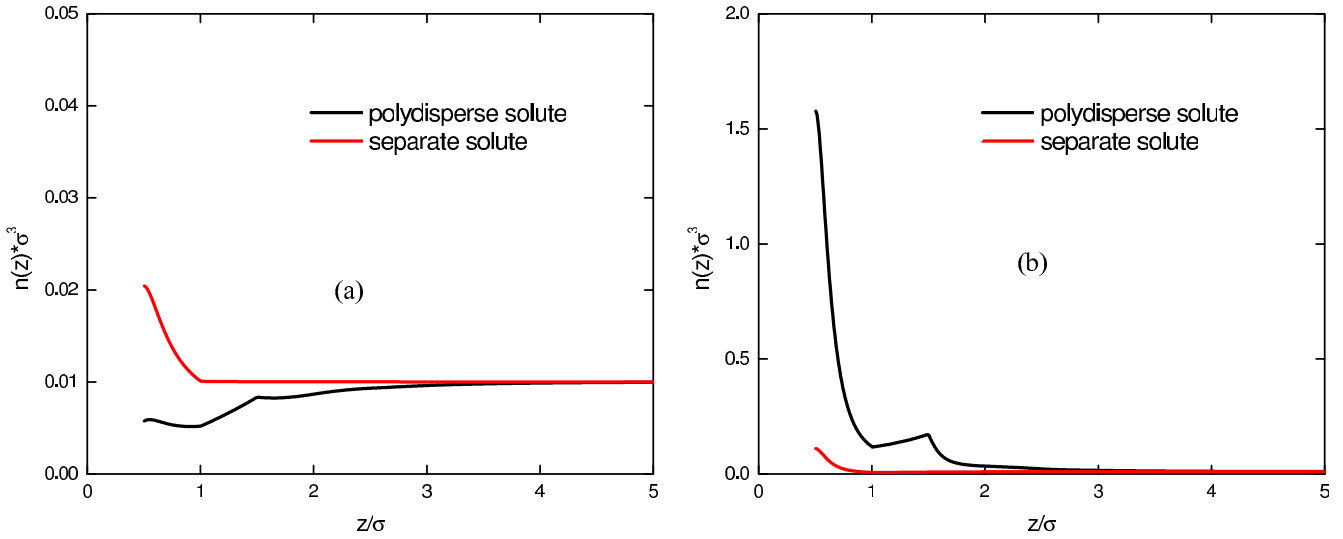

FIG. 7. Structural profiles of polydisperse and separate solute near an attractive surface at (a) $\epsilon_{wlj} = 0.5kT$ and (b) $\epsilon_{wlj} = 2.0kT$.

ensues from the fact that the monomers in the cationic chains no longer consist of branched oligomeric structures. The presence of the solvent does affect the steric term in the free-energy functional through the incompressibility assumption. We will assume that the solvent asserts itself in the spirit of a Bragg–Williams mixture, so that at every point the sum of the solvent and RTIL densities is fixed at some value, say n_0. However, in order to admit fluid structure, we use a "nonlocal" incompressibility assumption by coarse graining the RTIL contribution to the density. This has the effect of introducing a steric correlation term to the free-energy functional, which has the form

$$F_{\rm hs}[n_s(\mathbf{r})] = kT \int [n_0 - \bar{n}_s(\mathbf{r})](\ln[n_0 - \bar{n}_s(\mathbf{r})] - 1)\, d\mathbf{r}, \quad (28)$$

where $n_s(\mathbf{r})$ is the sum of cation and anion site densities,

$$n_s(\mathbf{r}) = n_c(\mathbf{r}) + n_a(\mathbf{r}), \quad (29)$$

and we have used the volume coarse graining [32],

$$\bar{n}_s(\mathbf{r}) = \frac{3}{4\pi\sigma^3} \int_{|r-r'|<\sigma} n_s(\mathbf{r}')dr'. \quad (30)$$

This notwithstanding the calculation of site densities follows the same procedures as outlined earlier, though now the polymeric structure of the cation chains has the simple form of a linear chain of tangential spheres [22]. In all cases considered below, the overall solution density was fixed at $n_0\sigma^3 = 0.7$ and the temperature was 294 K.

A. Adsorption transition of neutral systems

We begin our study by considering the RPM solution adjacent to a neutral surface but where the charges on the anion and cation species have been "switched off." The bulk ion density was set equal to $n_b\sigma^3 = \rho_b = 0.01$, and the average cation "polymerization" was given by $\langle L\rangle_b = 5$. This system is interesting, as it is known that, in the case of *ideal* monomers self-assembling into linear chains, an adsorption transition will occur at attractive surfaces, as the attractive surface energy approaches a critical value. Of course, our fluid species have a finite size, and it is known that the surface transition is suppressed when steric interactions are introduced between monomers. This notwithstanding, a sudden increase in the excess adsorption can occur at attractive enough surfaces, which is an echo of the adsorption transition in the ideal system. Instead of a sharp transition, the surface adsorption displays an inflection point corresponding to what can be referred to as a "soft" transition.

Instead of the full LJ surfaces considered earlier, here we model the surface as a hard wall plus a LJ attraction. The latter is translated so that particles at $z = \sigma/2$ are at the potential minimum. Thus we have

$$\omega_{wlj}(z) = 2\pi\epsilon_{wlj}\left[\frac{2}{45}\left(\frac{\sigma}{z+\Delta z}\right)^9 - \frac{1}{3}\left(\frac{\sigma}{z+\Delta z}\right)^3\right], \quad (31)$$

where $\Delta z = 0.358\sigma$. The attraction strength is ϵ_{wlj}.

In Fig. 7, we plot the density profiles of the associating (polydisperse) solute (the neutral "cation") and nonassociating (separate) solute (the neutral "anion") for a weak and a strong surface interaction. Qualitatively very different behavior is observed. At the smaller attractive potential $\epsilon_{wlj} = 0.5kT$, the adsorption of the polydisperse solute is actually lower than that of separate solute, as illustrated in Fig. 7(a). This can be attributed to the lower configurational entropy of the living polymers at the surfaces, leading to a depletion which cannot be overcome by a weak surface attraction.

At $\epsilon_{wlj} = 2.0kT$, however, the adsorption of the polydisperse chains dominates over that of the nonassociating separate solute [Fig. 7(b)]. As illustrated in Fig. 8(a), the adsorption of the polydisperse solute grows significantly with ϵ_{wlj}, due to cooperative adsorption of the bonded spheres. In contrast, the separate solute adsorption displays steady moderate growth with surface attraction. Eventually the adsorption by the polydisperse solute reaches a limit as determined by the incompressibility constraint.

Defining the excess adsorption $\Theta_{\rm ex}$ as

$$\Theta_{\rm ex} = \int_0^\infty [n(z) - n_b]\sigma^2\, dz, \quad (32)$$

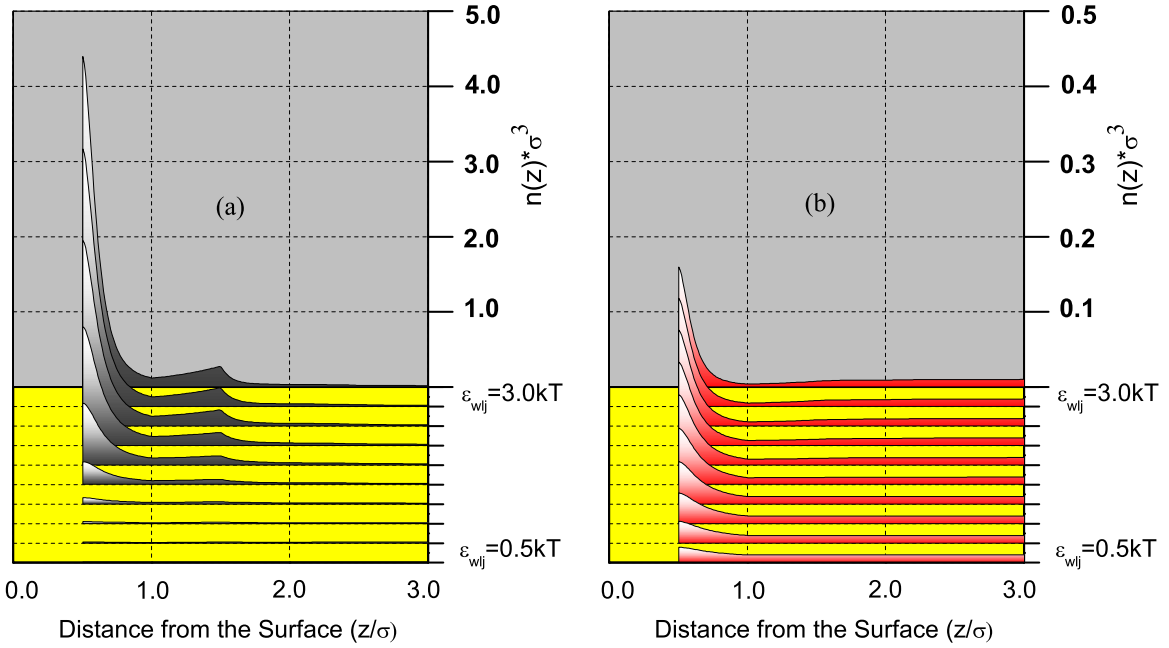

FIG. 8. Site density profiles of (a) polydisperse and (b) separate solute near a series of attractive surfaces. In the direction perpendicular to the paper, surface adsorption strength ranging from $\epsilon_{wlj} = 0.5kT$ to $\epsilon_{wlj} = 3.0kT$. The color gradient helps distinguish the different levels of adsorption density in each system.

we investigated how Θ_{ex} was influenced by the degree of polymerization in the bulk, $\langle L\rangle_b$, in Fig. 9(a). We found that the rapid increase in adsorption occurs at an earlier value of the adsorption strength when $\langle L\rangle_b$ is larger. This observation is consistent with the behavior of the ideal system of "living" polymers, where the adsorption transition occurs at a critical adsorption strength, which scales approximately as $\beta\epsilon^{\text{crit}}_{wlj} \approx \beta\epsilon^{0}_{wlj} + 1/\langle L\rangle_b^2$. Here ϵ^{0}_{wlj} is the surface strength that gives essentially zero excess adsorption. In addition to influencing the onset of the "soft" transition, we find that, at higher $\langle L\rangle_b$, the excess adsorption is consistently stronger, although this effect is rather weak in going from $\langle L\rangle_b = 5$ to $\langle L\rangle_b = 8$. Of course, in the limit $\langle L\rangle_b = 1$ the system becomes identical to a fluid of nonassociating ions.

The adsorption is magnified by reducing the bulk density of both solutes. As shown in Fig. 9(b), adsorption growth becomes much sharper at lower bulk density. This result is a reflection of the fact that the system becomes more ideal (reduced steric effect) as the bulk solute density is reduced. As expected, steric effects will eventually dominate at large adsorption strengths, and the excess adsorption approaches a constant.

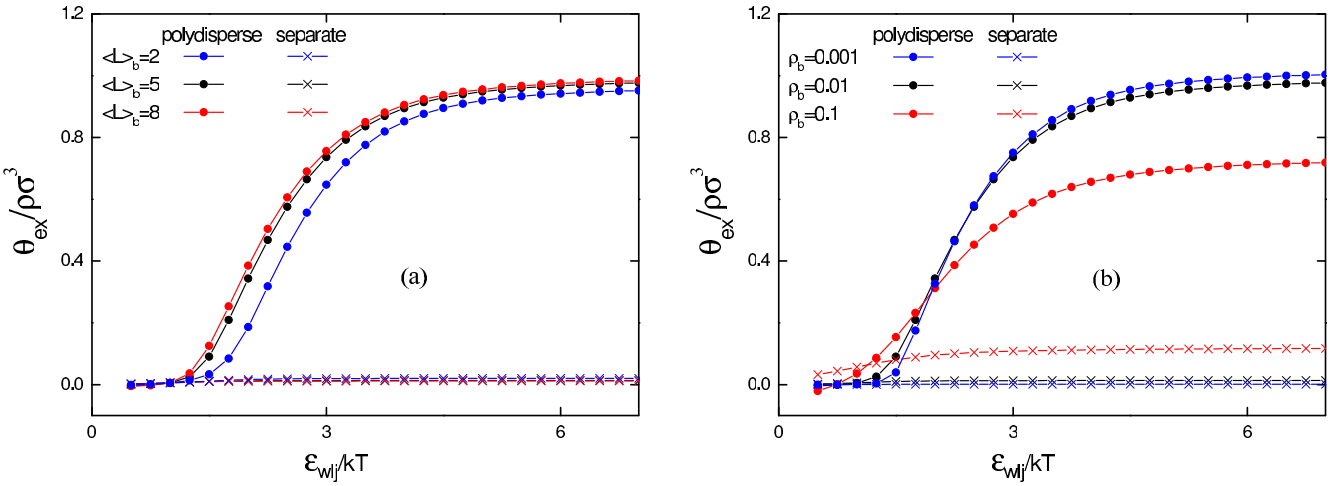

FIG. 9. Excess adsorption as a function of ϵ_{wlj} for polydisperse and separate species (a) at the same bulk concentration $\rho_b = 0.01$, but various degree of polymerization $\langle L\rangle_b = 2,5,8$ in bulk; (b) at the same degree of polymerization $\langle L\rangle_b = 5$ but various bulk solute concentrations $\rho_b = 0.001,0.01,0.1$.

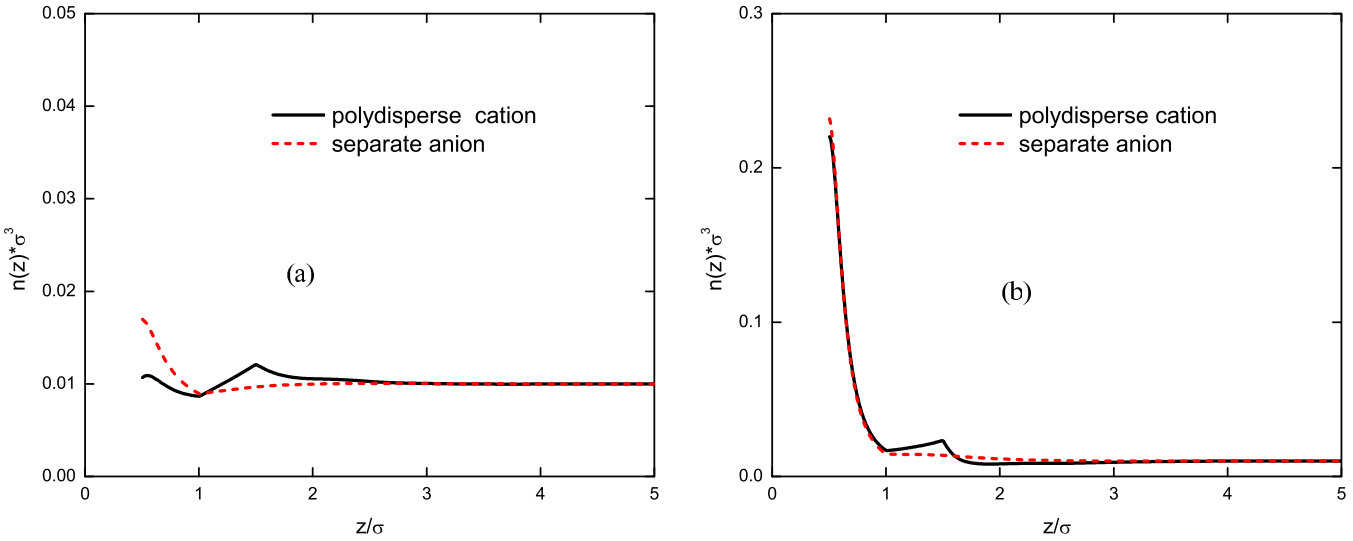

FIG. 10. Structural profiles of polydisperse cation and separate anion near a neutral attractive surface at (a) $\epsilon_{wlj} = 0.5kT$ and (b) $\epsilon_{wlj} = 2.0kT$.

B. Suppressed adsorption of charged systems

Our aim is to investigate if strong adsorption at electrodes, due to associating cations, will influence the electrical properties of dilute solutions of RTILs, so we now investigate the effect of charging up the solute species. In the following calculations we will adopt the bulk parameters $n_b\sigma^3 = 0.01$ and $\langle L\rangle_b = 5$, which gave rise to good adsorption characteristics in the neutral RPM model. The solvent was chosen to mimic water and had a relative dielectric constant, $\epsilon_r = 80$.

For charged solutes, electrostatic interactions are expected to play an important role, as charge separation is no longer possible to any great degree. Therefore, large excesses of cations on neutral surfaces, driven by cooperative adsorption, will be accompanied by essentially matching anion adsorption. This electroneutrality constraint is manifested in the free-energy functional via the mean-field expression for the electrostatic interactions, i.e., $F_{\rm elec}^{\rm MF}[n_c(\mathbf{r}),n_a(\mathbf{r}')]$ given by

$$F_{\rm elec}^{\rm MF}[n_c(\mathbf{r}),n_a(\mathbf{r}')] = \sum_{\alpha=a,c}\sum_{\beta=a,c}\frac{z_\alpha z_\beta e^2}{4\pi\epsilon_r\epsilon_0}\iint\frac{n_\alpha(\mathbf{r})n_\beta(\mathbf{r}')}{|\mathbf{r}-\mathbf{r}'|}\,d\mathbf{r}\,d\mathbf{r}'. \quad (33)$$

For the time being, we will ignore the correlation contributions due to the excess free-energy terms beyond the mean-field contribution These correlation terms are approximated using the mean spherical approximation [33,34], as embodied in the functional $F_{\rm elec}^{\rm MSA}[n_c(\mathbf{r}),n_a(\mathbf{r})]$,

$$F_{\rm elec}^{\rm MSA}[n_c(\mathbf{r}),n_a(\mathbf{r})] = F_{\rm elec}^{\rm MF}[n_c(\mathbf{r}),n_a(\mathbf{r})] - \frac{1}{2}\sum_{\alpha=a,c}\sum_{\beta=a,c}\iint n_\alpha(\mathbf{r})n_\beta(\mathbf{r}') \times\Delta C_{\alpha\beta}^{\rm elec}(|\mathbf{r}-\mathbf{r}'|)\,d\mathbf{r}\,d\mathbf{r}', \quad (34)$$

in which the excess direct correlation function $\Delta C_{\alpha\beta}^{\rm elec}(\mathbf{r})$ is derived in Ref. [34]. This *correlated* functional is expected to be better suited for a dilute fluid, as it is based on a rigorous second-order expansion of the free-energy functional [34,35].

Neglecting the $F_{\rm elec}^{\rm MSA}$ term amounts to a Poisson–Boltzmann treatment of an electrolyte solution with π-π associating cations.

Using the surface adsorption potential in Eq. (31), we computed the density profiles and excess adsorption of this electrostatically coupled system at a neutral surface. The density profiles at high and low adsorption strength are given in Fig. 10. At low surface attraction, the adsorption of the nonassociating anions is stronger than the associating cations due to entropic depletion, although the differences are smaller compared with the neutral fluid. As the surface attraction grows, the cation adsorption also increases. Unlike the neutral fluid, however, the growth of the cation density peak is impeded by the need for accompanying anions to maintain a degree of electroneutrality so as to ensure the free-energy penalty for charge separation is not too high. As anions do not possess the cooperative adsorption of the cations, the overall adsorption of both species is significantly damped. The similarity in the density profiles of anions and cations in this case vindicate the neglect of the $F_{\rm elec}^{\rm MSA}$ correlation contribution to the free energy. This is because the integration of the direct correlation function over locally similar but oppositely charged density profiles gives a small contribution to the excess chemical potential.

The behavior described above is also reflected in the excess adsorption curve, shown in Fig. 11, where, in contrast to the neutral fluid, the adsorption of anions and cations is identical. This occurs because the adsorption of both charged species requires charge neutrality, as the infinitely planar system cannot support a net adsorbed charge. We also see in Fig. 11 that a rapid increase in adsorption takes place at a higher adsorption strength for the charged fluid, in comparison with the neutral system. The adsorption of the cations (and anions) also saturates at roughly half the value in the neutral system. This is due to the fact that the total adsorption of fluid particles is dominated by steric effects, to which both anions and cations

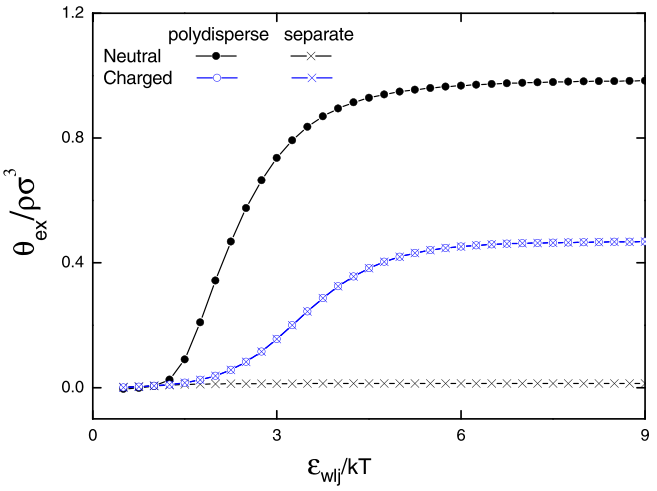

FIG. 11. Near a neutral surface, excess adsorption curve as a function of ϵ_{wlj} for polydisperse and separate species in both neutral [parameters from Fig. 9(a)] and charged systems. Bulk parameters are $\langle L\rangle_b = 5$ and $\rho_b = 0.01$.

contribute roughly equally in the charged fluid. In contrast, adsorption is mainly due to the associating species in the neutral case.

C. Adsorption transition induced by surface charges: Mean-field and correlated systems

We now consider the case of the associating RPM electrolyte adjacent to a charged electrode. The expected charge separation in this system makes it necessary to include electrostatic correlations via the $F_{\text{elec}}^{\text{MSA}}$ functional. The importance of the electrostatic correlation term is explicitly demonstrated below. Our aim is to investigate if a negatively charged electrode will cause a significant increase in surface adsorption of associating cations, compared with anions against positively charged electrodes. In this case, we expect this to lead to an asymmetric differential capacitance, which is larger at negative potential. As the electrode potential varies, studies have found that the differential capacitance of double layer is influenced by various factors, such as the structural asymmetry in ion shapes [36] and charge concentration [37]. Meanwhile, mixing composition of ionic liquids opens up new paths of improving electrochemical performance [38].

Similarly to the concept of surface binding energy [39], our DFT calculation has adjusted the attraction from the surface for a systemic comparison between associating and nonassociating species. We chose a LJ attraction strength of $\epsilon_{wlj} = 2.0k_BT$. In other words, the attraction is set slightly higher than the point at which adsorption begins to rapidly increase in the neutral fluid, Fig. 9(a).

We begin by assessing the importance of electrostatic correlations in describing the RTIL response to a negatively charged electrode. We did this by solving the DFT both with and without the $F_{\text{elec}}^{\text{MSA}}$ functional in the free energy. We chose a fairly high surface charge density of -20 Å$^2/e$ to emphasize the effects of these correlations. As shown in Fig. 12, the correlated system shows a much larger adsorption of cations adjacent to the negative electrode, compared with the mean-field system. Indeed, surface overcharging is apparent in the correlated solution, as suggested by the alternating layers of counterions and coions, which is not seen in the mean-field solution. This confirms our assertion that a correlated functional is especially important where stronger than usual cation adsorption is induced by π-π stacking.

In Fig. 13, we show typical adsorption profiles of the RTIL against both positive and negative surfaces at a lower absolute surface charge density of 80 Å$^2/e$. In both calculations, electrostatic correlations are included in the functional. Figure 13(a) shows a significantly higher adsorption of polydisperse cation against the negative surface than anions against the positive surface, Fig. 13(b). Interestingly, the large cation peak in Fig. 13(a) also attracts a higher anion adsorption

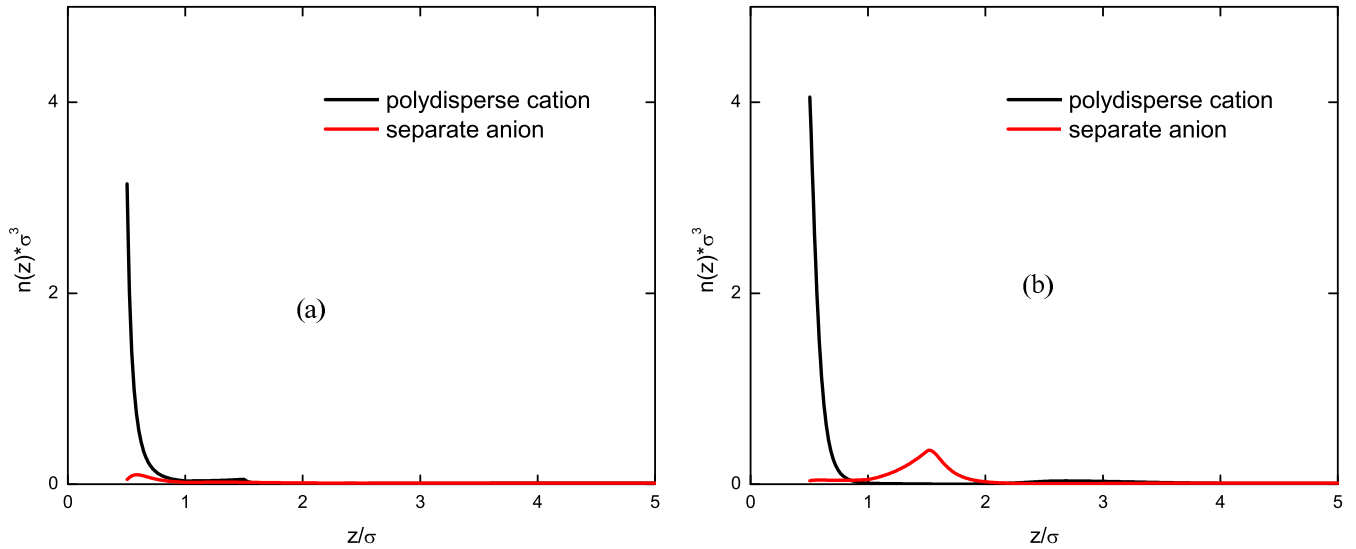

FIG. 12. Density profiles of associating cations and separate anions near a negatively charged surface at -20 Å$^2/e$ (a) mean-field system and (b) correlated system.

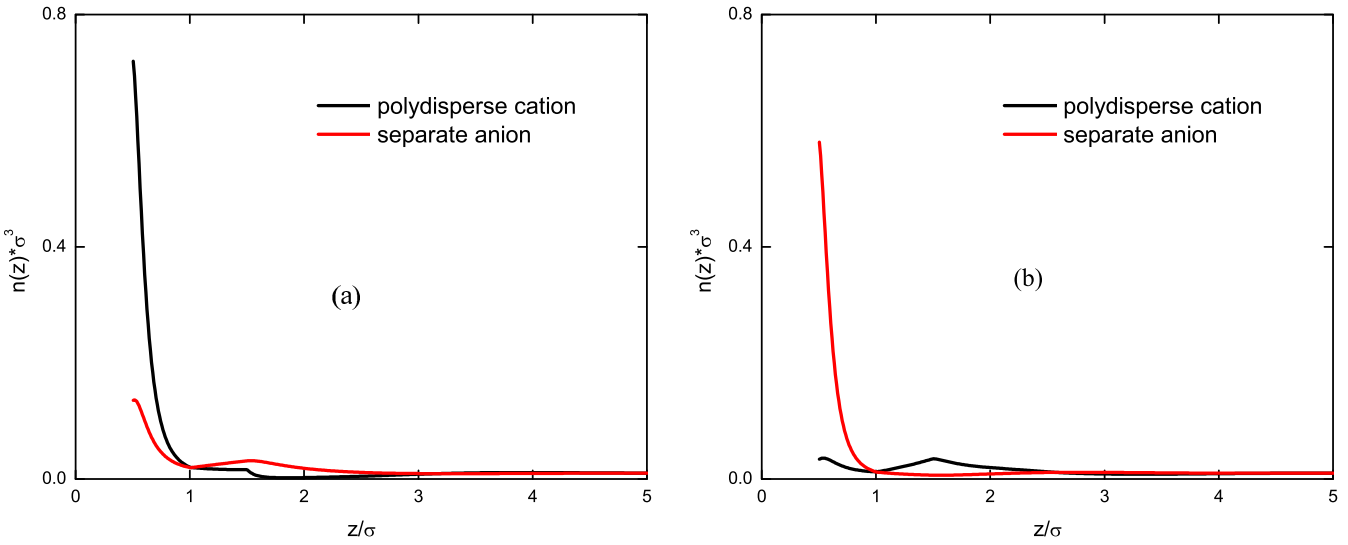

FIG. 13. Density profiles of associating cations and separate anions near (a) negative surface at -80 Å$^2/e$ and (b) positive surface at $+80$ Å$^2/e$.

close to the surface, as driven by the electrostatic and steric correlations.

In order to investigate how the electrode properties were influenced by cation association, we calculated the potential at a single electrode surface as a function of the surface charge density. For the purpose of a comprehensive comparison, we also considered an equivalent system where the cations are nonassociating.

In both sets of calculations we compared the DFT results for mean-field and correlated treatments of the electrostatic interactions. The results in Fig. 14 show that for both associating and nonassociating systems, the correlated functional gives smaller absolute surface potentials for a given charge density. For positive surface charges, the curves coincide for both associating and nonassociating systems (for both treatments at the mean-field and correlated level). This is because the nonassociating anions are responsible for the surface screening, while the cations, whether associating or not, play little role in this. In contrast, the potential curve is consistently lower in the associating system at negative surface charge density. Clearly, the associating cations are significantly more effective at screening the electrodes than the individual anions.

This is more apparent in the differential capacitance (DC) curves in Fig. 15, where we see enhanced capacitance at negative surface potentials due to cation association. This result indicates that asymmetry in the DC may not only be driven by different molecular architecture in anions and cations, but also specific interactions (such as π-π stacking) accompanying dispersion interactions to the surface may play a role in amplifying these effects.

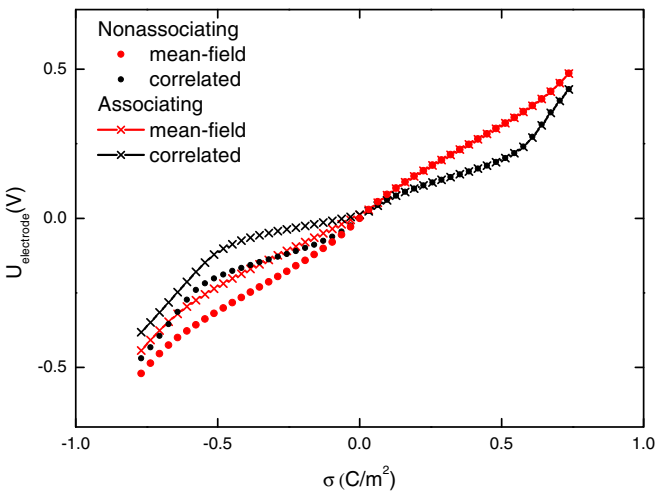

FIG. 14. Surface electrical potential as a function of surface charge density. Both mean-field and correlated cases are calculated for associating and nonassociating system.

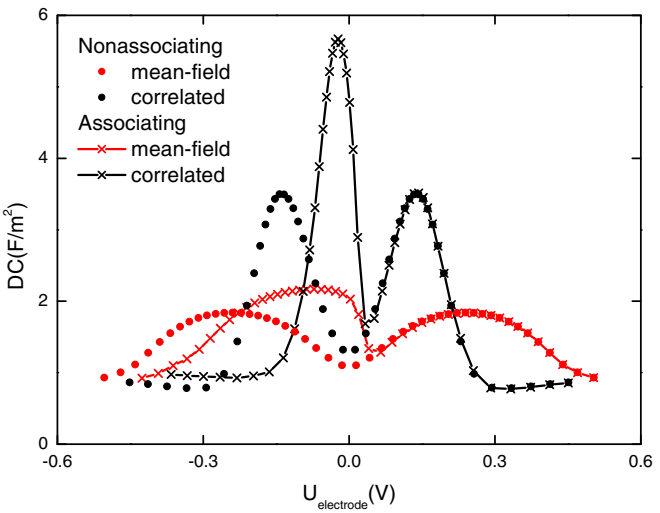

FIG. 15. Differential capacitance as a function of surface potential derived from data in Fig. 14.

V. CONCLUSIONS

In contrast to the study of cation–anion association into neutral pairs and higher-order clusters [1,2], we describe here the effect of a clustering of imidazolium-based cations, due to π-π stacking. We have generalized the density-functional theory of polydisperse polymers to the case where the associating monomers possess the multiple-branch architecture of RTILs. Such a theory will have wider applications in other polydisperse polymers and polyelectrolytes containing more complex intramolecular structure. The resulting structural profiles of the pure RTIL fluid remained very similar to that of the nonassociating RTILs model. Indeed, we found that adsorption to negatively charged electrodes by cations may be slightly weaker if they can also associate, due to polymer depletion effects. Subsequent work in the RTIL+solvent system shows that this will be especially the case if the surface has only a weak attraction to the monomers.

We explored RTIL+solvent mixtures using the restricted primitive model for the ionic liquid component in order to simplify our analysis. If the RTIL component is attracted to the surface via dispersion forces, then we find that in neutral systems (where the fluid charges are artificially set to zero) the excess adsorption of the solute grows rapidly with increasing surface adsorption strength beyond a critical value. This result echoes the sharp transition seen in ideal associating fluids at adsorbing surfaces.

When the charges are switched back on, however, electroneutrality dampens this "soft" transition, as the associating ions will need to be accompanied by counterions. This notwithstanding, we find that cation association does lead to a significantly enhanced differential capacitance at negative surface potentials, compared to positive potentials. This effect may be further amplified by a stronger dispersion attraction to the surfaces, which will be investigated in future work.

ACKNOWLEDGMENT

This work is supported by National Natural Science Foundation of China (Grant No. 21703153).

APPENDIX A: TURNING THE CATION MOLECULE INTO A SINGLE SITE MONOMER

In this Appendix section as well as two following sections, we present a complete picture the theoretical solution of site densities for the multibranched, polydisperse cation. In accordance with the model in Fig. 1, each cation molecule in a π-π associated chain of [C_4MIM^+] cations can be treated as a single site monomer, which we refer to as the π *bead* for convenience. The π bead has the same coordinate as the central bead in the charged star ($c3$) of the cationic molecule but carries excess chemical potential contributions from all the branches of the cation molecule that emerge from $c3$. Hence, the π bead becomes an "effective" particle which replaces a cation. Considering the branches attached to $c3$, the *effective* chemical potential for the π bead can be defined as

$$\lambda_\pi(\mathbf{r}) = \lambda_c(\mathbf{r}) + \ln[c(c2,\mathbf{r})c(c4,\mathbf{r})c(c9,\mathbf{r})c(c10,\mathbf{r})], \quad \text{(A1)}$$

where $\lambda_c(\mathbf{r})$ is the "bare" excess chemical potential of the $c3$ bead (which is the same as that for all positively charged beads)

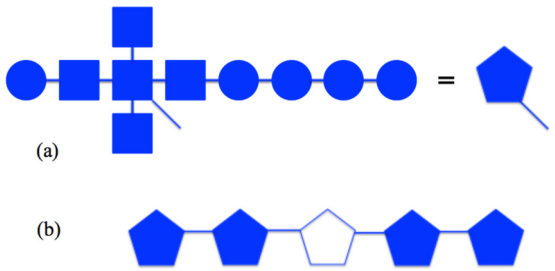

FIG. 16. (a) Diagrams representing the multibranch cation as a single π bead denoted by a pentagon. The solid line stemming from π bead represents the rigid bond of length σ. (b) Diagram for the normalized site density of the third π bead on a chain of five π beads, $n^\pi(3;5:\mathbf{r})/(\phi_p F(5))$.

and we have used the branch end segment distributions of the rest of the cation molecule. We now obtain the end segment distribution functions, $c^\pi(k,\mathbf{r})$, of a linear chain of π beads of length k. For example, we have, using $c^\pi(0,\mathbf{r}) = 1$,

$$c^\pi(1,\mathbf{r}) = \frac{e^{\lambda_\pi^b}}{4\pi\sigma^2}\int e^{-\lambda_\pi(\mathbf{r}')}c^\pi(0,\mathbf{r})\delta(|\mathbf{r}'-\mathbf{r}|-\sigma)\,d\mathbf{r}', \quad \text{(A2)}$$

which is given by the diagram in Fig. 16(a), where we have let the vertex of the π bead be represented by a pentagon. The quantity, λ_π^b, is the chemical potential of the π bead in the bulk, which is equal to λ_c^b. The recursion formula for end segment distributions is then

$$c^\pi(i+1,\mathbf{r}) = \frac{e^{\lambda_\pi^b}}{4\pi\sigma^2}\int e^{-\lambda_\pi(\mathbf{r}')}c^\pi(i,\mathbf{r}')\delta(|\mathbf{r}'-\mathbf{r}|-\sigma)\,d\mathbf{r}'. \quad \text{(A3)}$$

These end segment distributions can be used to generate the site densities of the π bead. For example, the normalized density of the $c3$ site due to the third cation of a chain of five associated cations is given by the diagram in Fig. 16(b), which in explicit terms is

$$n^\pi(3;5:\mathbf{r})/[\phi_p F(5)] = e^{\lambda_\pi^b-\lambda_\pi(\mathbf{r})}c^\pi(2,\mathbf{r})^2, \quad \text{(A4)}$$

where $\phi_p F(5)$ gives the bulk density of cation chains of length $L=5$ and $n^\pi(i;L:\mathbf{r})$ denotes the density of the $c3$ site due to the ith cation in a chain of L associated cations. The general formula for the $c3$ site density is given by

$$n^\pi(i;L:\mathbf{r}) = \phi_p F(L)e^{\lambda_\pi^b-\lambda_\pi(\mathbf{r})}c^\pi(i-1,\mathbf{r})c^\pi(L-i,\mathbf{r}). \quad \text{(A5)}$$

APPENDIX B: OBTAINING THE TOTAL $c3$ SITE DENSITY

The total density of the $c3$ site at any point in space is the same as the total π density, summed over all sites and the different lengths of π-π associated chains of cations. It is given by

$$n^\pi(\mathbf{r}) = \sum_{L=1}^{\infty}\sum_{i=1}^{L} n^\pi(i;L:\mathbf{r}). \quad \text{(B1)}$$

Substituting Eq. (A5) into Eq. (B1) gives the following:

$$n^{\pi}(\mathbf{r}) = \sum_{L=1}^{\infty}\sum_{i=1}^{L}\phi_p F(L) e^{\lambda_{\pi}^{b}-\lambda_{\pi}(\mathbf{r})} c^{\pi}(i-1,\mathbf{r}) c^{\pi}(L-i,\mathbf{r}). \tag{B2}$$

It is useful to define the related end segment distributions, $d^{\pi}(i,\mathbf{r})$, given by

$$d^{\pi}(i,\mathbf{r}) = e^{\frac{\lambda_{\pi}^{b}-\lambda_{\pi}(\mathbf{r})}{2}} c^{\pi}(i-1,\mathbf{r}) \tag{B3}$$

with

$$d^{\pi}(1,\mathbf{r}) = e^{\frac{\lambda_{\pi}^{b}-\lambda_{\pi}(\mathbf{r})}{2}}. \tag{B4}$$

The recursion formula for these new distributions can be written as

$$d^{\pi}(i+1,\mathbf{r}) = \int d^{\pi}(i,\mathbf{r}') T(\mathbf{r},\mathbf{r}')\, d\mathbf{r}', \tag{B5}$$

where $T(\mathbf{r},\mathbf{r}')$ is a connectivity kernel defined by

$$T(\mathbf{r},\mathbf{r}') = \frac{e^{\lambda_{\pi}^{b}}}{4\pi\sigma^2}\delta(|\mathbf{r}-\mathbf{r}'|-\sigma) e^{-\frac{\lambda_{\pi}(\mathbf{r})+\lambda_{\pi}(\mathbf{r}')}{2}}. \tag{B6}$$

The average density is then given by the following (more symmetric) equation:

$$n^{\pi}(\mathbf{r}) = \phi_p \sum_{L=1}^{\infty} F(L) \sum_{i=1}^{L} d^{\pi}(i,\mathbf{r}) d^{\pi}(L+1-i,\mathbf{r}). \tag{B7}$$

We will now introduce a specific form for the chain length distribution, $F(L)$. As stated earlier, we expect that the chains of associated cations should display the exponential distribution of a living polymer in the bulk. This is because the π-π interaction is essentially constant and acts between neighboring molecules, while the electrostatic interactions between the associated cations will be well screened. It is important to note that this distribution describes the chain lengths in the bulk fluid. In the case of the nonuniform fluid, say, near an electrode surface, the *local* length distribution will also be influenced by the excess chemical potentials of the sites in the molecules and will generally not be exponential. At this point, however, rather than choosing an exponential for $F(L)$, we will use a slightly more general functional form that is often used to describe polydispersity in polymeric systems. This is the well-known Schulz–Flory (SF) distribution, which describes a wider class of distributions including the exponential distribution of living polymers. The SF distribution can be expressed as

$$F(L) = NL^n e^{-\frac{L(n+1)}{\langle L\rangle_b}} \tag{B8}$$

with the normalization constant

$$N = \frac{(n+1)^{(n+1)}}{\Gamma(n+1)\langle L\rangle_b^{(n+1)}}, \tag{B9}$$

and where $\langle L\rangle_b$ is the average degree of polymerization in the bulk (where we have ignored the slight difference between averaging over discrete and continuous L). The quantity n determines the degree of polydispersity with the distribution becoming more monodispersed with n going to infinity. The case $n = 0$ corresponds to the exponential distribution of the living polymer system.

Using, $k = L + 1$, and defining

$$K = \frac{(n+1)^{(n+1)}}{\Gamma(n+1)\langle L\rangle_b^{(n+1)}} e^{\frac{(n+1)}{\langle L\rangle_b}}, \tag{B10}$$

we substitute Eq. (B8) into Eq. (B7) and get

$$\begin{aligned} n^{\pi}(\mathbf{r})(\phi_p K)^{-1} &= \sum_{k=2}^{\infty}\sum_{i=1}^{k-1}(k-1)^n e^{-k\frac{(n+1)}{\langle L\rangle_b}} d^{\pi}(i,\mathbf{r}) d^{\pi}(k-i,\mathbf{r}) \\ &= \sum_{k=2}^{\infty}\sum_{i=1}^{k-1}(i-1+k-i)^n e^{-i\frac{(n+1)}{\langle L\rangle_b}} d^{\pi}(i,\mathbf{r}) \\ &\quad \times e^{-(k-i)\frac{(n+1)}{\langle L\rangle_b}} d^{\pi}(k-i,\mathbf{r}) \\ &= \sum_{l=2}^{n}\sum_{m=0}^{l} A(l,m,n) \sum_{k=2}^{\infty}\sum_{i=1}^{k-1} i^m e^{-i\frac{(n+1)}{\langle L\rangle_b}} d^{\pi}(i,\mathbf{r}) \\ &\quad \times (k-i)^{(n-l)} e^{-(k-i)\frac{(n+1)}{\langle L\rangle_b}} d^{\pi}(k-i,\mathbf{r}), \end{aligned} \tag{B11}$$

where we have used a binomial expansion for the $(k-1)^n$ leading to the following assignments: $A(l,m,n) = {}^nC_l \times {}^lC_m(-1)^{l-m}$, with ${}^nC_l = \frac{n!}{(n-l)!l!}$.

To simplify Eq. (B11), we define the following transformation:

$$\hat{d}^{\pi}(k,r) = \sum_{i=1}^{\infty} i^k e^{-i\frac{(n+1)}{\langle L\rangle_b}} d^{\pi}(i,\mathbf{r}). \tag{B12}$$

Substituting Eq. (B12) into Eq. (B11) means that $n(\mathbf{r})$ can be rewritten as a sum of product functions as follows:

$$n^{\pi}(\mathbf{r})(\phi_p K)^{-1} = \sum_{l=2}^{n}\sum_{m=0}^{l} A(l,m,n)\hat{d}^{\pi}(n-l,\mathbf{r})\hat{d}^{\pi}(m,\mathbf{r}). \tag{B13}$$

Our goal now is to solve for the $\hat{d}^{\pi}(k,\mathbf{r})$ functions. After multiplying both sides of Eq. (B5) by $(i+1)^k e^{-(i+1)\frac{n+1}{\langle L\rangle_b}}$ and summing over i, we obtain

$$\begin{aligned} &\hat{d}^{\pi}(k,\mathbf{r}) - e^{-\frac{n+1}{\langle L\rangle_b}} d^{\pi}(1,\mathbf{r}) \\ &\quad = \sum_{i=1}^{\infty}(i+1)^k e^{-(i+1)\frac{n+1}{\langle L\rangle_b}} \int d^{\pi}(i,\mathbf{r}') T(\mathbf{r},\mathbf{r}') d\mathbf{r}' \\ &\quad = e^{-\frac{n+1}{\langle L\rangle_b}} \sum_{j=0}^{k} {}^kC_j \int \hat{d}^{\pi}(j,\mathbf{r}') T(\mathbf{r},\mathbf{r}') d\mathbf{r}', \end{aligned} \tag{B14}$$

which finally gives the following recursion relation for $\hat{d}^{\pi}(k,\mathbf{r})$:

$$e^{\frac{n+1}{\langle L\rangle_b}} \hat{d}^{\pi}(k,\mathbf{r}) = d^{\pi}(1,\mathbf{r}) + \sum_{j=0}^{k} {}^kC_j \int \hat{d}^{\pi}(j,\mathbf{r}') T(\mathbf{r},\mathbf{r}') d\mathbf{r}'. \tag{B15}$$

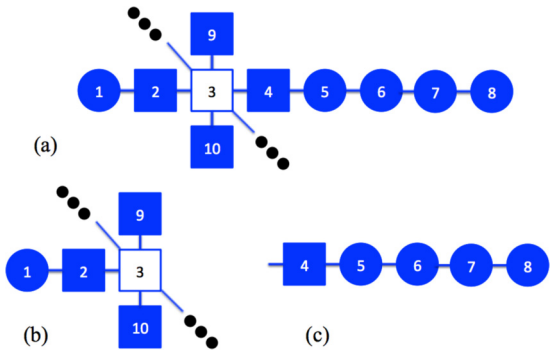

FIG. 17. Diagram for factoring the normalized site density at $c3$ into a chain backbone and a single branch term, (a) diagram for normalized $c3$ site density in a cation chain, (b) diagram of function $m^{\pi}(\mathbf{r})$, and (c) diagram for branch end segment distribution, $c(c4,\mathbf{r})$.

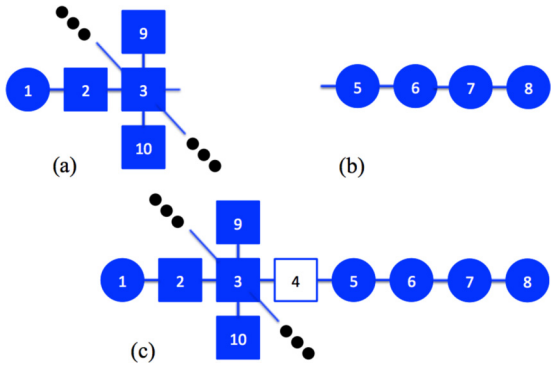

FIG. 18. Diagrams for solving site density of bead $c4$ by combining the contributions from (a) $m^{\pi}(\mathbf{r})$ diagram and (b) branch end segment distribution $c(5,\mathbf{r})$. (c) Normalized site density for $c4$ in a cation chain.

APPENDIX C: SOLVING SITE DENSITIES FOR THE REST OF THE BRANCHES

After obtaining the density of the π bead in Eq. (B13), the next step is to work out densities of the rest beads on the branches. Without loss of generality, we demonstrate the process of solving for the site density of bead $c4$ on the cation. The density of π beads is equal to the site density of the $c3$ bead, as shown in Fig. 17(a). It can be written as the product of the backbone of associating chain [Fig. 17(b)] and a single branch on which $c4$ resides [Fig. 17(c)]. Based on this interpretation, we can define the function $m^{\pi}(\mathbf{r})$ below

$$n^{\pi}(\mathbf{r}) = n_b^{(c)} m^{\pi}(\mathbf{r}) c(c4,\mathbf{r}), \tag{C1}$$

which implicitly contains contributions from chains of all lengths L, distributed according to $F(L)$. Note that $c(c4,\mathbf{r})$ is the usual branch end segment distribution on the cation and thus the unknown $m^{\pi}(\mathbf{r})$ is readily obtained. Figure 18(a) shows how a complementary end segment distribution can be constructed from $m^{\pi}(\mathbf{r})$. This can then be used to construct the site densities on the molecular branch containing $c4$. For example, Fig. 18(c) gives the normalized overall site density for bead $c4$,

$$n_{c4}(\mathbf{r})/n_b = \frac{e^{\lambda_c^b - \lambda_c(\mathbf{r})}}{4\pi\sigma^2} \int m^{\pi}(\mathbf{r}')\delta(|\mathbf{r}-\mathbf{r}'|-\sigma)\, d\mathbf{r}' c(5,\mathbf{r}). \tag{C2}$$

Site densities for other beads along the branch can be easily determined by propagating towards the end of chain.

While we began with the intention of deriving a DFT for associating ions, the methodology derived above is more general, allowing us to treat much more complicated systems, such as branched polyelectrolytes with polydispersity. Furthermore, it is clear that association or polymerization of the anion moiety can also be treated in a similar fashion. However, we will focus for now on the system of π-π associated cations, which is expected to follow a SF distribution corresponding to $n = 0$ in Eq. (B8),

$$F(L) = \frac{1}{\langle L\rangle_b} e^{-\frac{L}{\langle L\rangle_b}}. \tag{C3}$$

[1] K. Ma, J. Forsman, and C. E. Woodward, J. Chem. Phys. **142**, 174704 (2015).
[2] K. Ma, J. Forsman, and C. E. Woodward, J. Phys. Chem. C **121**, 1742 (2017).
[3] A. G. Avent, P. A. Chaloner, M. P. Day, K. R. Seddon, and T. Welton, J. Chem. Soc. Dalton Trans. **1994**, 3405 (1994).
[4] Y. Zhou, J. H. Schattka, and M. Antonietti, Nano Lett. **4**, 477 (2004).
[5] E. Buisine, K. de Villiers, T. J. Egan, and C. Biot, J. Am. Chem. Soc. **128**, 12122 (2006).
[6] F. Tang, T. Ohto, T. Hasegawa, M. Bonn, and Y. Nagata, Phys. Chem. Chem. Phys. **19**, 2850 (2017).
[7] K. Subramaniam, A. Das, and G. Heinrich, Composites Sci. Technol. **71**, 1441 (2011).
[8] E. Bosch, C. L. Barnes, N. L. Brennan, G. L. Eakins, and B. E. Breyfogle, J. Org. Chem. **73**, 3931 (2008).
[9] H.-F. Chen, W.-Y. Hung, S.-W. Chen, T.-C. Wang, S.-W. Lin, S.-H. Chou, C.-T. Liao, H.-C. Su, H.-A. Pan, P.-T. Chou, Y.-H. Liu, and K.-T. Wong, Inorg. Chem. **51**, 12114 (2012).
[10] J. P. Quirino, P. Anres, J. Sirieix-plénet, N. Delaunay, and P. Gareil, J. Chromatogr., A **1218**, 5718 (2011).
[11] M. Brüssel, M. Brehm, A. S. Pensado, F. Malberg, M. Ramzan, A. Stark, and B. Kirchner, Phys. Chem. Chem. Phys. **14**, 13204 (2012).
[12] R. P. Matthews, T. Welton, and P. A. Hunt, Phys. Chem. Chem. Phys. **17**, 14437 (2015).
[13] H. Weber and B. Kirchner, J. Phys. Chem. B **120**, 2471 (2016).
[14] H. Weber, O. Hollóczki, A. S. Pensado, and B. Kirchner, J. Chem. Phys. **139**, 123 (2013).
[15] A. Mele, G. Romano, M. Giannone, E. Ragg, G. Fronza, G. Raos, and V. Marcon, Angew. Chem. **45**, 1123 (2006).
[16] R. P. Matthews, T. Welton, and P. A. Hunt, Phys. Chem. Chem. Phys. **16**, 3238 (2014).
[17] B. Freasier, C. Woodward, and S. Nordholm, J. Chem. Phys. **90**, 5657 (1989).

[18] K. Ma, J. Forsman, and C. E. Woodward, J. Phys. Chem. C **118**, 15825 (2014).
[19] J. Z. Wu, Aiche J. **52**, 1169 (2006).
[20] J. Z. Wu, T. Jiang, D. E. Jiang, Z. H. Jin, and D. Henderson, Soft Matter **7**, 11222 (2011).
[21] J. Forsman, C. E. Woodward, and M. Trulsson, J. Phys. Chem. B **115**, 4606 (2011).
[22] C. E. Woodward, J. Chem. Phys. **94**, 3183 (1991).
[23] J. Forsman, C. E. Woodward, and B. C. Freasier, J. Chem. Phys. **117**, 1915 (2002).
[24] K. Ma, X. Wang, J. Forsman, and C. E. Woodward, J. Phys. Chem. C **121**, 13539 (2017).
[25] D. Henderson, S. Lamperski, Z. Jin, and J. Wu, J. Phys. Chem. B **115**, 12911 (2011).
[26] D. E. Jiang, D. Meng, and J. Z. Wu, Chem. Phys. Lett. **504**, 153 (2011).
[27] M. Granfeldt, S. Miklavic, S. Marcelja, and C. Woodward, Macromolecules **23**, 4760 (1990).
[28] C. Woodward and B. Jönsson, Chem. Phys. **155**, 207 (1991).
[29] R. P. Sear, J. Chem. Phys. **111**, 2255 (1999).
[30] J. Forsman and C. E. Woodward, Soft Matter **8**, 2121 (2012).
[31] R. Szparaga, C. E. Woodward, and J. Forsman, J. Phys. Chem. C **116**, 15946 (2012).
[32] S. Nordholm, M. Johnson, and B. C. Freasier, Aust. J. Chem. **33**, 2139 (1980).
[33] Z. Li and J. Wu, J. Phys. Chem. B **110**, 7473 (2006).
[34] Y. X. Yu, J. Wu, Y. X. Xin, and G. H. Gao, J. Chem. Phys. **121**, 1535 (2004).
[35] Z. Li and J. Wu, Phys. Rev. Lett. **96**, 048302 (2006).
[36] D. Henderson, W. Silvestre-Alcantara, M. Kaja, S. Lamperski, J. Wu, and L. B. Bhuiyan, J. Mol. Liq. **228**, 236 (2017).
[37] D. Henderson, S. Lamperski, L. Bari Bhuiyan, and J. Wu, J. Chem. Phys. **138**, 144704 (2013).
[38] C. Lian, K. Liu, K. L. Van Aken, Y. Gogotsi, D. J. Wesolowski, H. L. Liu, D. E. Jiang, and J. Z. Wu, ACS Energy Lett. **1**, 21 (2016).
[39] K. Liu, C. Lian, D. Henderson, and J. Wu, Mol. Phys. **115**, 454 (2017).